Two-dimensional curved panel vibration
and flutter analysis in the frequency and time domain
under thermal and in-plane load

Hamid Moosazadeh[*1] and Mohammad M. Mohammadi[2a]

1Department of Aerospace Engineering, Tarbiat Modares University, Tehran, 14115-143, Iran
2Faculty of mechanics, Malek Ashtar University of technology, Iran

Abstract. The analysis of nonlinear vibrations, buckling, post-buckling, flutter boundary determination and post-flutter behavior of a homogeneous curved plate assuming cylindrical bending is conducted in this article. Other assumptions include simply-supported boundary conditions, supersonic aerodynamic flow at the top of the plate, constant pressure conditions below the plate, non-viscous flow model (using first- and third-order piston theory), nonlinear structural model with large deformations, and application of mechanical and thermal loads on the curved plate. The analysis is performed with constant environmental indicators (flow density, heat, Reynolds number and Mach number). The material properties (i.e., coefficient of thermal expansion and modulus of elasticity) are temperature-dependent. The equations are derived using the principle of virtual displacement. Furthermore, based on the definitions of virtual work, the potential and kinetic energy of the final relations in the integral form, and the governing nonlinear differential equations are obtained after fractional integration.

This problem is solved using two approaches. The frequency analysis and flutter are studied in the first approach by transferring the handle of ordinary differential equations to the state space, calculating the system Jacobin matrix and analyzing the eigenvalue to determine the instability conditions. The second approach discusses the nonlinear frequency analysis and nonlinear flutter using the semi-analytical solution of governing differential equations based on the weighted residual method. The partial differential equations are converted to ordinary differential equations, after which they are solved based on the Runge–Kutta fourth- and fifth-order methods. The comparison between the results of frequency and flutter analysis of curved plate is linearly and nonlinearly performed for the first time. The results show that the plate curvature has a profound impact on the instability boundary of the plate under supersonic aerodynamic loading. The flutter boundary decreases with growing thermal load and increases with growing curvature.

Keywords: curved plate; first-order piston theory; in-plane load; panel flutter; thermal load; 2D plate

1. Introduction

From the aeroelastic point of view, studying the effect of curvature and plate vibrations are of great importance. Even a small geometric curvature on a homogeneous plate is crucial to

---

*Corresponding author, Ph.D., E-mail: hamid.moosazadeh@modares.ac.ir.
a Assistant Professor, E-mail: Mohammadi.mm@mut.ac.ir.

determine the aeroelastic behavior (with regard to the range of flutter instability), buckling and vibrations of plates.

Plates may have a general and irreversible curvature. The structure may suffer a general or local imperfection as a result of the production process and operations. Curvatures are also found in the location of plate connections in different forms (welds, rivets, etc.). Geometric curvatures markedly affect the speed of flutter. Static loading due to the aerodynamic flow in front of the curved plate significantly impacts the flutter boundaries. The amplitude of plate oscillation in the flutter conditions is in the range of plate curvature. A curvature is applied to the strain energy of the structure, which reduces or increases the structural stiffness.

The overall curvature can be matched to the buckling mode or vibration modes of the plate. The curvature size clearly affects the nonlinear transient response of the plate. It should be noted that the plate vibration frequency depends on the curvature height value.

Yang *et al*. (2012) investigated the flutter of thermally buckled finite element panels. The finite element formulation was extended to treat the flutter model of a semi-infinite panel which is buckled into large deflections due to aerodynamic thermal load. Birman *et al*. (1990) studied the effect of aerodynamic heating on the deflection of composite cylindrical panels in fluid flow. It was shown that the main contributor to large static deformations is non-uniform aerodynamic heating, while aerodynamic pressure is of secondary significance at high Mach numbers.

Nydick *et al*. (1995) studied the hypersonic flutter on curved panels. The flutter of shallow curved heated three-dimensional (3D) orthotropic panels exposed to hypersonic flow was considered. A comparison of the aerodynamic loads predicted by the third-order piston theory, Euler equations and Navier Stokes equations was also presented. Krause *et al*. (1998) studied the influence of curvature on supersonic panel flutter. The effect of curvature on flutter boundaries and flutter behavior was investigated for isotropic two-dimensional (2D) and 3D panels exposed to supersonic flow on one side of the panel using the finite element method (FEM). Librescu *et al*. (2002) studied the supersonic/hypersonic flutter and post-flutter of geometrically non-perfect circular cylindrical panels. An analysis of the flutter and post-flutter of infinitely-long thin-walled circular cylindrical panels in a supersonic/hypersonic flow was also presented. The third-order piston theory and shock wave aerodynamics were used in conjunction with the geometrically nonlinear shell theory to obtain the aeroelastic equations.

Pany *et al*. (2003) inspected the flutter of periodically-supported curved panels. They considered one-dimensional axial wave propagation in an infinitely long periodically-supported cylindrical curved panel subjected to supersonic airflow. The aerodynamic forces were based on the piston theory. Azzouz *et al*. (2004) used FEM to simulate the nonlinear flutter of shallow shells under yawed supersonic flow. A nonlinear finite element formulation was employed to analyze the effects of arbitrary flow angle on large-amplitude supersonic flutter of isotropic and composite shallow shell panels.

Azzouz *et al*. (2005) utilized FEM for the nonlinear flutter of cylindrical shell panels under yawed supersonic flow. A finite element frequency domain technique and a multi-modal finite element time domain method were developed to predict the flutter and the nonlinear flutter response of shallow shell panels. Fazelzadeh studied the chaotic behavior of nonlinear curved panels in supersonic flow. Chaotic and hyper-chaotic behavior were detected using qualitative and quantitative methodologies such as time history, phase portrait, Lyapunov exponents and fractal dimension. Singha and Mandal examined the supersonic flutter characteristics of composite cylindrical panels. The effects of curvature, laminate stacking sequence, airflow direction and boundary condition on the supersonic flutter characteristics of laminated composite cylindrical shell panels were also investigated.

Ghoman *et al*. (2009) used a time-domain method to study the nonlinear flutter of curved panels under yawed supersonic flow at elevated temperatures. Time history responses, phase plots, power spectrum density and bifurcation diagrams were employed to understand the pre/post-flutter behavior of cylindrical panels of different heights under increasing dynamic pressure and uniform or linearly-varying static thermo-aerodynamic loading (STAL).

Abbas *et al*. (2011) studied the supersonic/hypersonic flutter behavior of aero-thermo-elastic geometrically-imperfect curved skin panel. The aero-thermo-elastic governing equations were developed from the geometrically-imperfect nonlinear theory of infinitely-long 2D curved panels. Yang *et al*. (2012) proposed an aero-thermo-elastic two-way coupling method for hypersonic curved panel flutter. The governing equations of a simply-supported 2D curved panel were derived based on the von Kármán geometrically-nonlinear theory. Compared with the results of one-way aero-thermal-elastic coupling, it was shown that the two-way coupling, which decreases the flight time with respect to the onset of flutter, is more dangerous.

Amirzadegan and Dowell (2020) studied the flutter and post-flutter limit cycle oscillation (LCO) of elastic shells in supersonic regime. The effects of streamwise and spanwise curvature were shown to be different, with the former lowering the stability and the latter increasing the stability.

Amirzadegan *et al*. (2019) studied the flutter behavior of isotropic plates in view of pre-stress effects. Zhou *et al*. (2019) examined the panel flutter considering the thickness changes, boundary conditions, and the length to width ratio. Cao *et al*. (2019) examined the panel flutter assuming thermal effects to determine the Hopf-bifurcation. Muc *et al*. (2019) investigated the optimization of plate and shell structures under the influence of the flutter.

The first part of this paper is devoted to the frequency analysis of the vibrations and flutter of flat and curved plates. The second part deals with the time-domain analysis of nonlinear vibrations and post-flutter behavior of flat and curved plates. The combined effects of in-plane mechanical loads, uneven heat on the plate with temperature-dependent properties and supersonic aerodynamic loads, is first applied to a 2D curved plate. The results show that the flutter instability as well as the buckling of the plate and the shell displays a complex behavior due to the combined mechanical and thermal loads. The effect of in-plane compressive force demonstrates the complex behavior of panel flutter and the nonlinear frequency changes of structure. The use of an aerodynamic model based on the third-order piston theory makes the flutter boundary more critical.

2. Problem formulation

The model of curved panel under the effects of supersonic aerodynamic flow, in-plane load and aerodynamic heating is shown in Fig. 1.

The parameters displayed in Fig. 1 are as follows. U_∞: free flow velocity on the curved plate, R_x: in-plane load, P^d: dynamic flow pressure above the plate, P^s: low static pressure, T: flow temperature, h: thickness, H: maximum height of curvature, $\underline{R}_x$: radius of curvature, a: plate width.

Nonlinear finite element analysis is used to verify the vibrational behavior of the plate model with the effects of curvature. In this analysis, an initial displacement is applied to the structure and a static analysis is performed. Then, the free vibration analysis of the plate is performed in the presence of initial residual stresses. To investigate the nonlinear vibration frequencies of the structure, a fast Fourier transform (FFT) analysis of the dynamic free vibration response of the
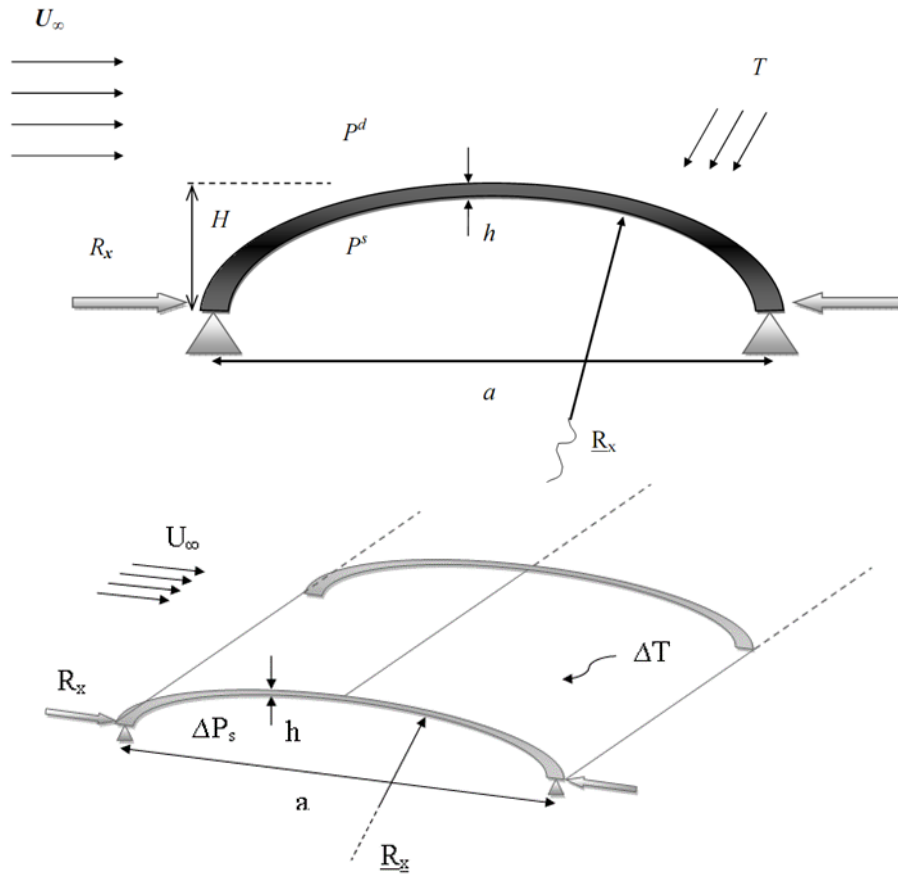
Fig. 1 2D plate geometry with environmental loads
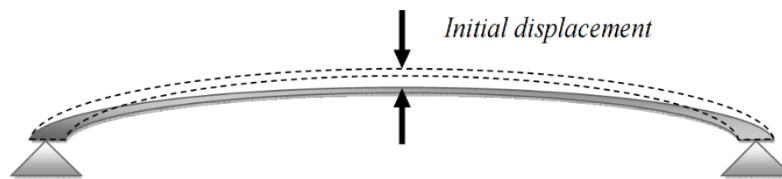
Fig. 2 Initial deformation in the transient analysis

system is employed. Accordingly, an initial displacement is exerted to the 2D plate model and after static analysis, transient vibrations under the pre-stress effect are investigated. Fig. 2 shows the initial plate displacement.

2.1 Structural formulation

The equations are derived taking the effect of aerodynamic heating into account with the use of virtual work. The virtual work principle in dynamic form is defined as Reddy (2003)

$$0 = \int_0^T (\delta U + \delta V - \delta K) dt \tag{1}$$

where δU, δV and δK are the virtual strain energy, the virtual work done by applied forces and the virtual kinetic energy, respectively, and are expressed as Reddy (2003)

$$\delta U = \int_V \overleftrightarrow{\sigma} : \delta \overleftrightarrow{\varepsilon} \ dV \tag{2}$$

$$\delta V = \int_{\Omega_0} \mathbf{p} . \delta \vec{\mathbf{u}} \ dx dy \tag{3}$$

$$\delta K = \int_V \rho \vec{\mathbf{u}}_{,t} . \delta \vec{\mathbf{u}}_{,t} \ dV \tag{4}$$

where $\overleftrightarrow{\sigma}$, $\overleftrightarrow{\varepsilon}$, $\vec{\mathbf{p}}$, $\vec{\mathbf{u}}$ and $\vec{\mathbf{u}}_{,t}$ are the stress tensor, strain tensor, external distributed force vector, displacement vector, and velocity vector, respectively, and Ω_0 is the mid-plane. Next, using the classical panel strain-displacement, Euler-Lagrange equations are derived. The structural equations are reduced from two dimensions to one dimension for a panel of infinite length. The structural bending equation is defined as Abbas *et al.* (2011) and Yang *et al.* (2012).

$$M_{x,xx} - N_x \left(w_{0,xx} - \frac{1}{\underline{R_x}} \right) + \varDelta P_a + M_{x,xx}^T + \rho_m h w_{0,tt} = 0 \tag{5}$$

where $w_0(x,t)$ is the plate's out-of-plane displacement, N_x is the in-plane axial force resultant, M_x and M_x^T are the bending and thermal moments resultant, $\varDelta P_a$ is the aerodynamic pressure, $\rho_m h w_{0,tt}$ is the panel transverse inertia and $\underline{R_x}$ is the curvature radius. Additionally, $M_x \equiv D w_{0,xx}$ and $D = Eh^3 / 12(1 - v^2)$ where D is the panel stiffness, E is the elastic modulus, v is the Poisson's ratio and $w_{0,xx}$ is the mid-plane curvature variation. The panel strain is defined via the nonlinear von Kármán relation as $\varepsilon_x = u_{0,x} + 1/2 \left(w_{0,x} \right)^2 + w_0 / R_1$ Reddy (2003). In aerospace applications such as airplane wings, fuselage or tail, the plate is connected rigidly to the aircraft structure. The stress is generated on the panel boundaries due to the existence of supports. The axial stress, N_x, is the total in-plane load in the x direction which is defined as Yang *et al.* (2012)

$$N_x = N_x^m + N_x^g + N_x^T \tag{6}$$

where N_x^m is the mechanical tensile or compressive load, N_x^g stems from curvature and nonlinear terms, and N_x^T is the in-plane thermal load. These terms are defined as

$$N_x^m = \frac{ah}{(1 - v^2) \int_0^a E(x)^{-1} dx} \eta \tag{7}$$

$$N_x^g = \frac{h}{(1 - v^2) \int_0^a E(x)^{-1} dx} \left(\frac{1}{2} \int_0^a \left(w_{0,x} \right)^2 dx + \frac{1}{\underline{R_x}} \int_0^a w_0 \ dx \right) \tag{8}$$

$$N_x^T = -\frac{1}{(1-v^2)}\frac{1}{\int_0^a E(x)^{-1}dx}\left((1+v)\int_0^a \alpha(x)\int_{-h/2}^{h/2}\Delta T\, dzdx\right) \tag{9}$$

The effect of thermal moment is expressed as Reddy (2003)

$$M_x^T = \frac{1}{(1-v)}\frac{\alpha(x)}{\int_0^a E(x)^{-1}dx}\left(\int_{-h/2}^{h/2}\Delta Tz\, dz\right) \tag{10}$$

where η is the tensile or compressive force coefficient per unit area on panel boundaries and ΔT is the rise in panel temperature with respect to the stress-free state (reference temperature T_{ref}). In fact, a linear temperature distribution across the panel thickness is assumed as $\Delta T(x,z) = T - T_{ref} = T_0(x) + zT_1(x)$ (Abbas *et al.* 2011, Gee and Sipcic 1999). At high speeds, the panel temperature rises to high values and reaches several hundreds of Celsius degrees. This leads to a reduction in flutter boundary and an increase in the LCO amplitude of the panel at the same dynamic pressure. The thermal effect is included in panel equations for subtle panel flutter modeling.

The temperature distribution for high velocity flights is assumed to be in the steady state while temperature variation along the thickness is disregarded. Hence, $\Delta T(x) = T_0(x)$ and, as a result, the in-plane thermal moment is neglected. The panel temperature is described by $T_0(x) = \overset{*}{T}\sin(\pi(x/a))$ where $\overset{*}{T}$ is the maximum in-plane temperature when $x = a/2$. Simply-supported boundary conditions are defined as $w_0(x,t) = 0$ and $w_{0,xx}(x,t) = 0$, (Miller *et al.* 2011). Material properties including elastic modulus E and thermal expansion coefficient α are assumed to be temperature-dependent as in (Muc *et al.* 2019)

$$E = E_0 + E_1 T_0 = E_0(1 + e_T T_0)\ , \qquad e_T = E_1/E_0 < 0$$
$$\alpha = \alpha_0 + \alpha_1 T_0 = \alpha_0(1 + \alpha_T T_0)\ , \qquad \alpha_T = \alpha_1/\alpha_0 > 0 \tag{11}$$

where e_T and α_T are the thermal variation coefficients for E and α. Thermoelastic coefficients of the material depend on the position and temperature. Therefore, $E = E(x,T)$ and $\alpha = \alpha(x,T)$.

2.2 Aerodynamic loading

Fluid-structure interaction is modeled based on the nonlinear piston theory. ΔP_a is the distributed pressure on the panel due to aerodynamic flow over the panel according to $\Delta P_a = P^d(x,t) + P^s(x)$ where $P^d(x,t)$ is the effect of unsteady aerodynamic force and $P^s(x)$ is the initial static aerodynamic force. Assuming an isentropic pressure on the panel and using the piston theory based on the downwash velocity V_z in one dimension, one can write (Epreaunu *et al.* 2019)

$$P^d(x,t) = P_\infty\left(1 + \gamma\frac{M}{\beta_1}\left(\eta_1\frac{V_z}{c_\infty}\right)\right) \tag{12}$$

where c_∞ is the sound speed and γ is the isentropic gas constant. Based on a third-order expansion of Equation (9), the third-order piston theory is derived as

$$P^d(x,t) = P_\infty \left(1 + \gamma \frac{M}{\beta_1}\left(\eta_1 \frac{V_z}{c_\infty}\right) + \left[\frac{\gamma\ (\gamma+1)}{4}\right]\frac{M}{\beta_1}\left(\eta_1 \frac{V_z}{c_\infty}\right)^2 + \frac{\gamma\ (\gamma+1)}{12}\frac{M}{\beta_1}\left(\eta_1 \frac{V_z}{c_\infty}\right)^3\right) \tag{13}$$

where $\eta_1 = M/\sqrt{M^2 - 1}$, and $c_\infty^2 = \gamma P_\infty/\rho_\infty$ in which P_∞, ρ_∞ and U_∞ are the atmospheric pressure, air density and free-stream steady velocity, respectively. Also, $\gamma = 1.4$.

In order to define the aerodynamic pressure on the panel, the downwash velocity (V_z) due to fluid flow over the panel is defined based on the panel vertical deflection as in (Yang *et al.* 2012)

$$V_z = \left(\beta_2 w_{0,t} + U_\infty(w_{0,x} + \widehat{w}_{0,x})\right) \tag{14}$$

where $\widehat{w}_{0,x}$ is the effect of initial imperfection or curvature on the panel. The piston theory is a conventional method for aeroelastic analysis of a system in supersonic and hypersonic flows. The fluid flow only exists above the panel while the flow velocity below the panel is zero. For the Mach number M, the dynamic pressure q_∞, and constants β_1 and β_2, the following relations are taken into account: $M = U_\infty/c_\infty$, $q_\infty = \rho_\infty U_\infty^2/2$, $\beta_1 = \sqrt{M^2 - 1}$, $\beta_2 = M^2 - 2/M^2 - 1$. For high Mach numbers, $\beta_1 = M$ and $\beta_2 = 1$.

2.3 Nonlinear aero-thermo-elastic equations of the panel

The non-dimensional system variables are defined according to

$$W = \frac{w}{a}\ ,\quad \widehat{W} = \frac{\widehat{w}}{h}\ ,\quad \xi = \frac{x}{a}\ ,\quad \bar{t} = t\Omega_0\ ,\quad \Omega_0 = \left(\frac{\pi}{a}\right)^2\sqrt{\frac{D_0}{\rho_m h}}\ ,\quad \bar{\Omega} = \Omega_0\frac{a}{c_\infty}\ ,\quad K = \frac{\omega}{\Omega_0},$$

$$\bar{h} = \frac{h}{a}\ ,\quad \hat{h} = \frac{h}{R_x}\ ,\quad \bar{P}^s(x) = P^s(x)\frac{a^4}{D_0 h}\ ,\quad T_{cr} = \frac{D_0}{Eha^2\alpha_0}\ ,\quad \bar{\rho} = \frac{\rho_m}{\rho_\infty}\ ,\quad H \approx \frac{a^2}{8R_x}\ , \tag{15}$$

$$\tau = \frac{T}{T_{cr}}\ ,\quad \bar{T} = \tau\ \sin(\pi\xi)\ ,\quad \mu = \frac{\rho_\infty a}{\rho_m h}\ ,\quad \beta = \sqrt{M^2 - 1}\ ,\quad \lambda = \frac{2qa^3}{\beta D_0},\ R_x = \frac{E_0 ha^2\bar{\eta}_1}{D_0(1-v^2)} = C_r\pi^2$$

where C_r is the in-plane load coefficient and R_x is the magnitude of in-plane load. Using the non-dimensional quantities and substituting them in the above equations, the final nonlinear aero-thermo-elastic equation of the 2D panel is obtained as

$$(1 + \delta_e e_T T_{cr}\tau\sin(\pi\xi))W_{,\xi\xi\xi\xi} - \left(1\Big/\left(\int_0^1 \frac{d\xi}{1 + \delta_e e_T T_{cr}^*\tau\sin(\pi\xi)}\right)\right)\times$$

$$\frac{12}{\bar{h}^2}\left(\eta + \frac{1}{2}\int_0^1 (W_{,\xi})^2 d\xi + \frac{\hat{h}}{\bar{h}}\int_0^1 W d\xi\right)\left(W_{,\xi\xi} - \frac{\hat{h}}{\bar{h}}\right) -$$

$$\left(1\Big/\left(\int_0^1 \frac{d\xi}{1 + \delta_e e_T T_{cr}\tau\sin(\pi\xi)}\right)\right)\left(\frac{1}{1-v}\int_0^1 \left(1 + \delta_\alpha \alpha_T T_{cr}\tau\sin(\pi\xi)\right)\tau\sin(\pi\xi)d\xi\right)\times$$

$$\left(W_{,\xi\xi} - \frac{\hat{h}}{\bar{h}}\right) + \pi^4 W_{,\bar{t}\bar{t}} + \frac{M^2\pi^4}{\bar{h}\bar{\rho}\bar{\Omega}^2\beta_1}\eta_1\left(C_{a1}\left(\beta_2\frac{\bar{\Omega}}{M}W_{,\bar{t}} + W_{,\xi} + \bar{h}\widehat{W}_{,\xi}\right) + \right. \tag{8}$$

$$C_{a3}\frac{1+\gamma}{4}\eta_1 M\left(\beta_2\frac{\bar{\Omega}}{M}W_{,\bar{t}} + W_{,\xi} + \bar{h}\widehat{W}_{,\xi}\right)^2 + C_{a3}\frac{1+\gamma}{12}\eta_1^2 M^2\times$$

$$\left.\left(\beta_2\frac{\bar{\Omega}}{M}W_{,\bar{t}} + W_{,\xi} + \bar{h}\widehat{W}_{,\xi}\right)^3\right) = \bar{P}^s$$

where δ_e is the temperature-dependent modulus of elasticity and δ_α is the temperature-dependent coefficient of thermal expansion, which are taken as zero or one.

The effect of curvature is defined using (Abbas *et al.* 2011)

$$\widehat{w}/_H = \left[1 - (x - {}^a/_2)^2/({}^a/_2)^2\right] \tag{17}$$

The above equation is transformed into $\widehat{W} = -(\frac{\hat{h}}{2\bar{h}^2})\xi(\xi - 1)$.

2.4 Galerkin method

The Galerkin method is implemented to solve the integro-differential equation (Eq. (13)) so as to evaluate the structural response and the curvature impact on flutter boundary with thermoelastic properties. Moreover, simply-supported boundary conditions ($W = W_{,\xi\xi} = 0, \xi = 0,1$) are considered. The mode shape functions are defined such that the boundary conditions are satisfied:

$$W(\xi,\bar{t}) = \sum_{i=1}^{n} a_i(\bar{t})\,\phi_i(\xi) \tag{18}$$

$$\phi_i(\xi) = \sin(\lambda_i\xi) \ , \qquad \lambda_i = i\pi$$

Obviously, the approximate solution is not equal to the exact solution, and residual terms will remain. After multiplying the residual term or error by the proposed base function for the system mode shapes $\phi_r(\xi) = \sin(r\pi\xi), r = 1,2,\ldots,n$, integrating along the span and setting the result to zero, a series of ordinary differential equations are derived according to the number of expanded terms.

The mode shape functions with fixed support conditions are written as

$$\phi_i(\xi) = \sinh(\beta_i\xi) - \sin(\beta_i\xi) + \frac{(\sinh(\beta_i) - \sin(\beta_i))}{\cos(\beta_i) - \cosh(\beta_i)} \times (\cosh(\beta_i\xi) - \cos(\beta_i\xi)) \tag{19}$$

$$\cos\ (\beta_i)\cosh(\beta_i) - 1 = 0$$

Equating the residual weight ratio to zero results in

$$R_e = \int_0^1 F(\xi,\bar{t})\ \ \phi_r(\xi)d\xi = 0 \tag{20}$$

2.5 Converting equations into state-space form

A series of nonlinear ordinary differential equations (ODEs) are transformed into the state-space form and the Jacobian matrix is calculated. Using the resulting matrix, an eigenvalue analysis is performed, and the frequencies and damping of the system are plotted to show instability conditions. In the eigenvalue analysis, the structure frequencies are affected by thermal and mechanical loads. The system aeroelastic frequencies are also studied in order to inspect flutter and divergence. The results of such a frequency analysis are investigated for the first time and new aspects of the behavior of curved structure under different loads are shown in separate and combined forms.

To transform the first four natural modes of the structure, the equations are written as (Kouchkzadeh *et al.* 2010)

$$
\begin{aligned}
\ddot{a}_1 &= \dot{x}_5 \\
\ddot{a}_2 &= \dot{x}_6 \\
\ddot{a}_3 &= \dot{x}_7 \\
\ddot{a}_4 &= \dot{x}_8
\end{aligned}
\qquad
\begin{aligned}
\dot{a}_1 &= x_5 = \dot{x}_1 \\
\dot{a}_2 &= x_6 = \dot{x}_2 \\
\dot{a}_3 &= x_7 = \dot{x}_3 \\
\dot{a}_4 &= x_8 = \dot{x}_4
\end{aligned}
\qquad
\begin{aligned}
a_1 &= x_1 \\
a_2 &= x_2 \\
a_3 &= x_3 \\
a_4 &= x_4
\end{aligned}
\tag{21}
$$

Also, the Jacobian matrix is written in the form

$$
A = \begin{bmatrix}
\partial\dot{x}_1/\partial x_1 & \partial\dot{x}_1/\partial x_2 & \cdots & \cdot & \partial\dot{x}_1/\partial x_8 \\
\partial\dot{x}_2/\partial x_1 & \partial\dot{x}_2/\partial x_2 & \cdots & \cdot & \partial\dot{x}_2/\partial x_8 \\
\cdot & \cdot & \cdots & \cdot & \cdot \\
\cdot & \cdot & \cdots & \cdot & \cdot \\
\cdot & \cdot & \cdots & \cdot & \cdot \\
\cdot & \cdot & \cdots & \cdot & \cdot \\
\partial\dot{x}_8/\partial x_1 & \cdot & \cdots & \partial\dot{x}_8/\partial x_7 & \partial\dot{x}_8/\partial x_8
\end{bmatrix}
\tag{22}
$$

One can obtain eigenvalues using equation determinants as in

$$
|A - \lambda I| = 0 \tag{23}
$$

Thus, the final polynomial equation of degree 8 is generated as

$$
s_8\lambda^8 + s_7\lambda^7 + s_6\lambda^6 + s_5\lambda^5 + s_4\lambda^4 + s_3\lambda^3 + s_2\lambda^2 + s_1\lambda^1 + s_0 = 0 \tag{24}
$$

The coefficients s_0 to s_8 depend on the mechanical force inside the plate η_1, the heat inside the plate τ, the Mach number M, the height of plate curvature $\hat{h}$ and the thermal coefficient A_2. These terms are specified in Appendix. In general, one can write

$$
s_i = f(M, \hat{h}, \tau, A_2) \tag{25}
$$

By solving the resulting polynomial equation, the stability conditions and the shell stability boundary are determined.

3. Verification

A numerical validation of the proposed approach is provided here. Figure 3 illustrates the effect of curvature on the non-dimensional flutter dynamic pressure. The results obtained from the present analysis using six modes show very good agreement to the four-mode solution of Amirzadegan *et al.* (2019) and the eight-mode solution of Abbas *et al.* (2019).

For a nonlinear flat plate with the effect of in-plane load, the present study is compared with Epureanu's research (Amirzadegan *et al.* 2019). For the compressive load coefficient, -2.8, the LCO diagram is shown in Figure 4. The results of the code are fully consistent with Epureanu's research.

4. Numerical results

The results are explained in two sections. First, the frequency analysis of the curved panel structure is considered. The effect of plate curvature on frequency variations under in-plane load is studied. The aero-thermo-elastic analysis of curved panel is discussed in the second section. The
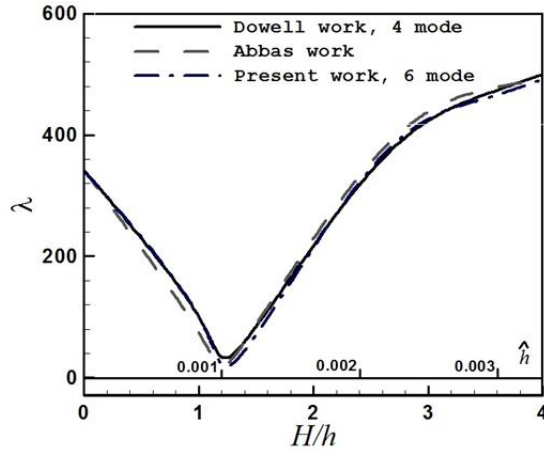
Fig. 3 Comparison of non-dimensional flutter dynamic pressure versus curvature ratio
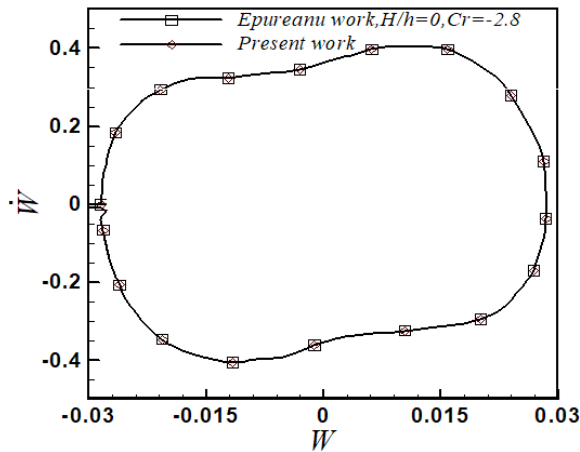
Fig. 4 Comparison of the results of the LCO of a nonlinear flat plate with the effect of internal load, with a coefficient of -2.8

Table 1 Plate properties

$\rho_m = 2700$ kg/m^3	$\alpha_0 = 5.7623e-6$ $1/k°$	$a = 1$
$\nu = 0.33$	$\alpha_T = 6.074e-4$ $1/k°$	$h = 0.01$
$E_0 = 70$ Gpa	$e_T = -6.941e-4$ $1/k°$	$C_\infty = 340$ m/s
$E_s = 1.183E_0 = 82.86$ Gpa	$\rho_\infty = 1.225$ kg/m^3	$\gamma = 1.4$

effect of plate curvature along with different environmental loads on the instability behavior of the plate is also investigated. The initial excitation condition for the first mode is assumed to be 0.1. Next, the results obtained from the present analysis using four, six and eight modes are compared.

Aluminum is the material of choice for the 2D curve panel. The mechanical properties and geometric parameters as well as flow field characteristics are shown in Table 1.

(a) Frequency domain   (b) Time domain (analytical and FEM)
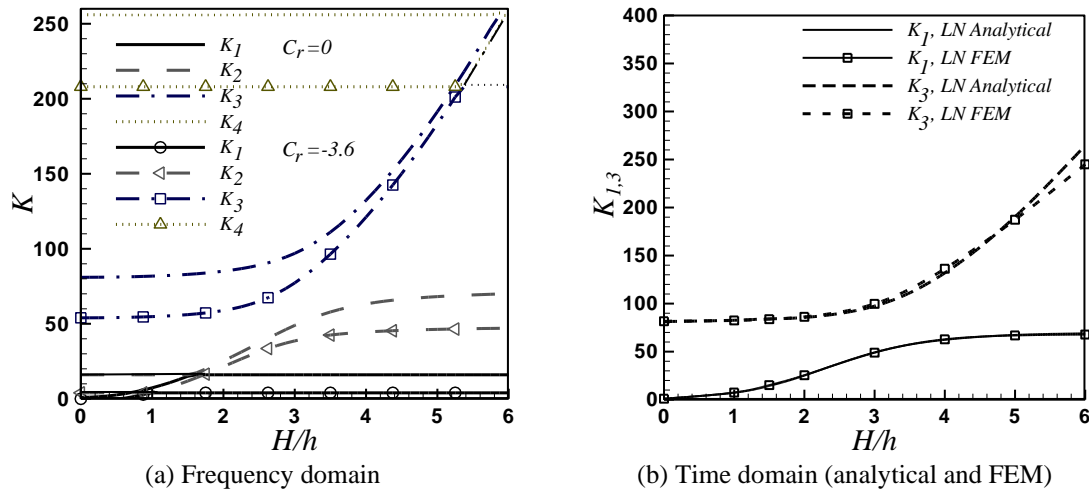
Fig. 5 Comparison of the first to fourth frequencies of curved plate for the in-plane load coefficients 0 and −3.6

4.1 Structural analysis of the curved panel

The results of this section consist of two parts. The first part is the analysis of structural dynamics in both frequency and time domains to determine the vibrational behavior of the structure under the effect of small and large initial excitations. Also, the effect of environmental conditions on the vibrational behavior of the curved panel in the frequency and time domains with the assumption of linear and nonlinear structures is investigated. In the second part, the aeroelastic and thermo-aero-elastic behavior of the curved plate in the frequency and time domains are examined and compared.

The comparison of the first to fourth frequencies of the curved plate for the curvature ratio of zero to 6, and for the in-plane load coefficients of 0 and −3.6, is shown in Fig. 5(a). The diagram shows the frequency domain analysis and the increase of the first and third frequencies with increasing plate curvature. The rise in compressive force inside the plate reduces the frequencies. Figure 5b compares the frequency domain and time domain analysis using the finite element and analytical methods, which shows a complete adaptation of the process of changing frequencies with the frequency domain results for small excitation.

Fig. 6(a) shows the nonlinear frequency changes of the plate in terms of curvature for the excitation conditions 0.0001 to 0.01. As the plate curvature increases, the first frequency of the structure also increases (except for the excitation 0.002). As the excitation grows, the frequency behavior of the plate changes from increasing to uniform with increasing curvature effect. Figure 6b compares the change in the first and second frequencies of the plate in terms of curvature for the analytical and the nonlinear finite element model. As observed, a good agreement is observed between these cases.

A comparison between the frequency changes of the flat and curved plate structure for curvatures 0, 2, 4 and 6 is performed for the first three modes. As shown in Fig. 7(a), the first frequency for zero curvature reaches zero at a pressure coefficient of −1. The second frequency for the zero pressure factor starts from 16 and reaches zero for the pressure factor of 4. The second frequency of the plate with zero curvature is equal to the first frequency of the curved plate with

(a) Initial conditions 0.0001 to 0.01   (b) Nonlinear analytical and FEM
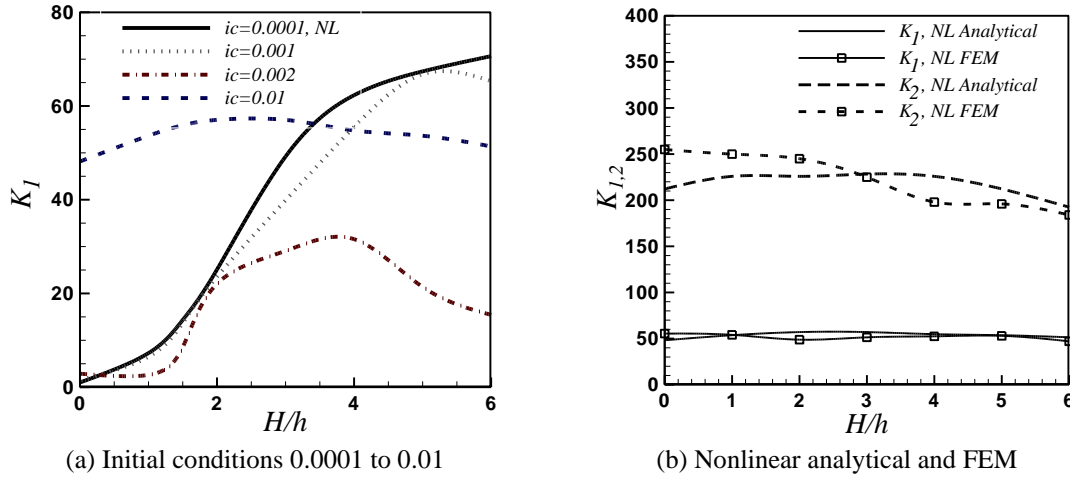
Fig. 6 Comparison of linear and nonlinear frequency changes of curved plate in terms of curvature change from 0 to 6

(a) *H/h* = 0 & 2   (b) *H/h* = 4 & 6
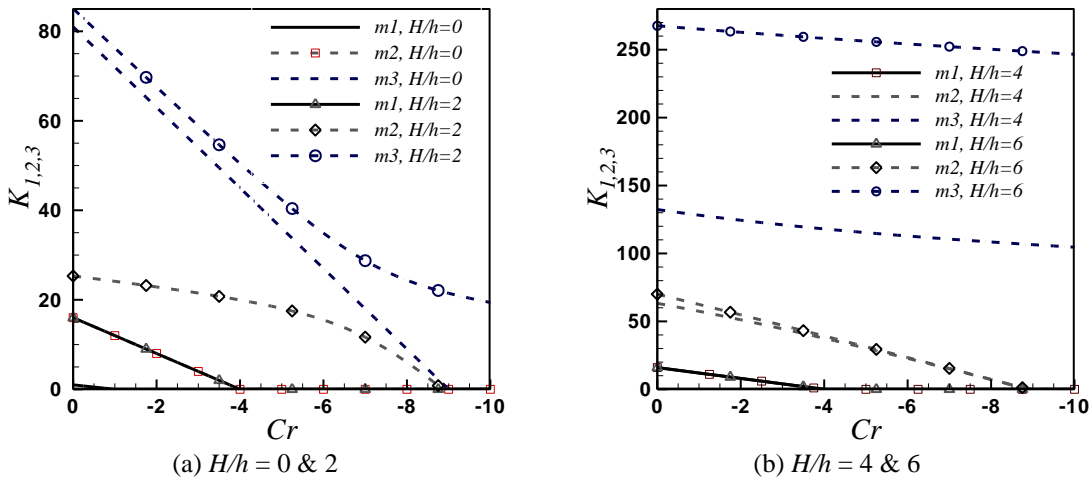
Fig. 7 Frequencies of the first to third modes of the flat and curved plate with respect to compressive force

the curvature 2. The frequency changes of the flat structure are uniform, whereas for the curved plate, the second and third frequency reductions have a curved shape, while the trend of changes in the second and third frequency is different. With increasing curvature of the structure from zero to 2, the first and second frequencies increase significantly.

For higher values of compressive force coefficient, the frequency difference between the equivalent flat and curved plate modes with a curvature of 2 grows. For the curvature ratios 4 and 6, as shown in Fig. 7(b), the first frequency of the structure is the same and the second and third frequencies of the structure slightly increase for the curvature ratio of 6. Comparing the curved plate frequency for the curvature ratios 2, 4 and 6 shows that as the compressive force coefficient increases, the first frequencies remain the same, while the second frequency of the plate with the curvature 2 shows more deviations compared with those of the plate with the curvatures 4 and 6. The frequency difference in the third mode increases for different curvatures.

(a) different initial condition

(b) Mode numbers 1 to 3 for the initial condition 0.003
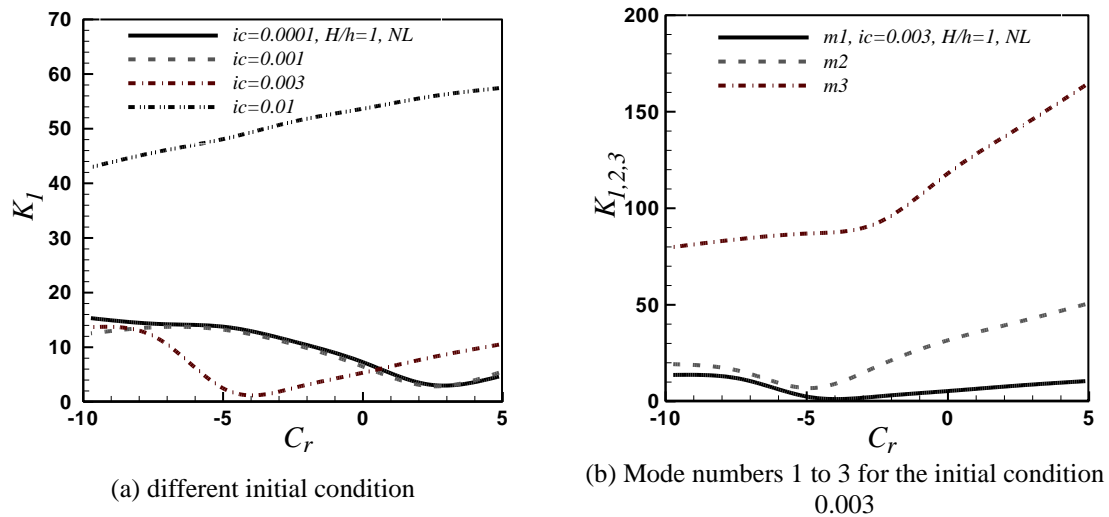
Fig. 8 Frequency versus compressive load coefficient for *H/h* = 1

With an increase in the camber ratio from 2 to 6 with respect to the in-plane load, the first frequency remains similar while the frequency difference is more visible at higher mode numbers. Frequency variation of higher camber ratios is more linear unlike that of lower camber ratios.

Fig. 8(a) shows the changes in the first frequency of the curved plate with a curvature of 1 for the initial excitation conditions 0.0001 to 0.01 in terms of the force inside the plate. The diagram is based on the nonlinear analysis of the structure. With increasing initial excitation, the system dynamic behavior and the frequency variation start to vary. By changing the in-plane load from tensile to compressive, for small excitation of the system, first the frequency reduction to the buckling limit is shown, then the frequency increase in the post-buckling range is specified. With a large increase in initial excitation, due to the increase in frequency and stiffness of the structure, a constant decrease in frequency is diverge, and the frequency in the specified compressive load range does not approach the buckling conditions. Therefore, regarding the nonlinear analysis, the effect of excitation on the dynamic behavior of the curved plane is quite evident. Also, the diagram for *ic* = 0.003 corresponds well with the analysis diagram in the frequency domain up to the buckling boundary where the linear behavior of the structure is visible, and the results in both analyses confirm each other. Figure 8b shows the frequency changes of the first to third modes of the curved plate for the excitation 0.003. All three frequencies have a decreasing trend until the buckling limit is reached at a load factor of −5, after which the post-buckling behavior and increasing frequencies are observed.

The nonlinear frequency analysis of the curved plate structure under the initial excitation of 0.01 is performed in the time domain and the structure vibrations are investigated in this section. Figs. 9(a)-9(d) show the vibrations of the plate with the curvatures 0, 1, 3 and 5. In Fig. 9(a), for the flat plate, the symmetrical vibration with respect to the equilibrium state of the plate is shown in the range of 0.02 > W > −0.02. Fig. 9(b) shows the dimensionless oscillation of the plate with a curvature of 1, asymmetrically with respect to the equilibrium state, in the range 0.02 > W > −0.04. In Fig. 9(c), the plate oscillation for the curvature 3 is in the range 0.02 > W > −0.065. Finally, for the curvature 5 in Fig. 9(d), the oscillation amplitude is in the range 0.02 >W > −0.1 and the oscillating behavior is irregular. Thus, as the plate curvature increases, the vibrations

(a) *H/h = 0*   (b) *H/h = 1*

(c) *H/h = 3*   (d) *H/h = 5*
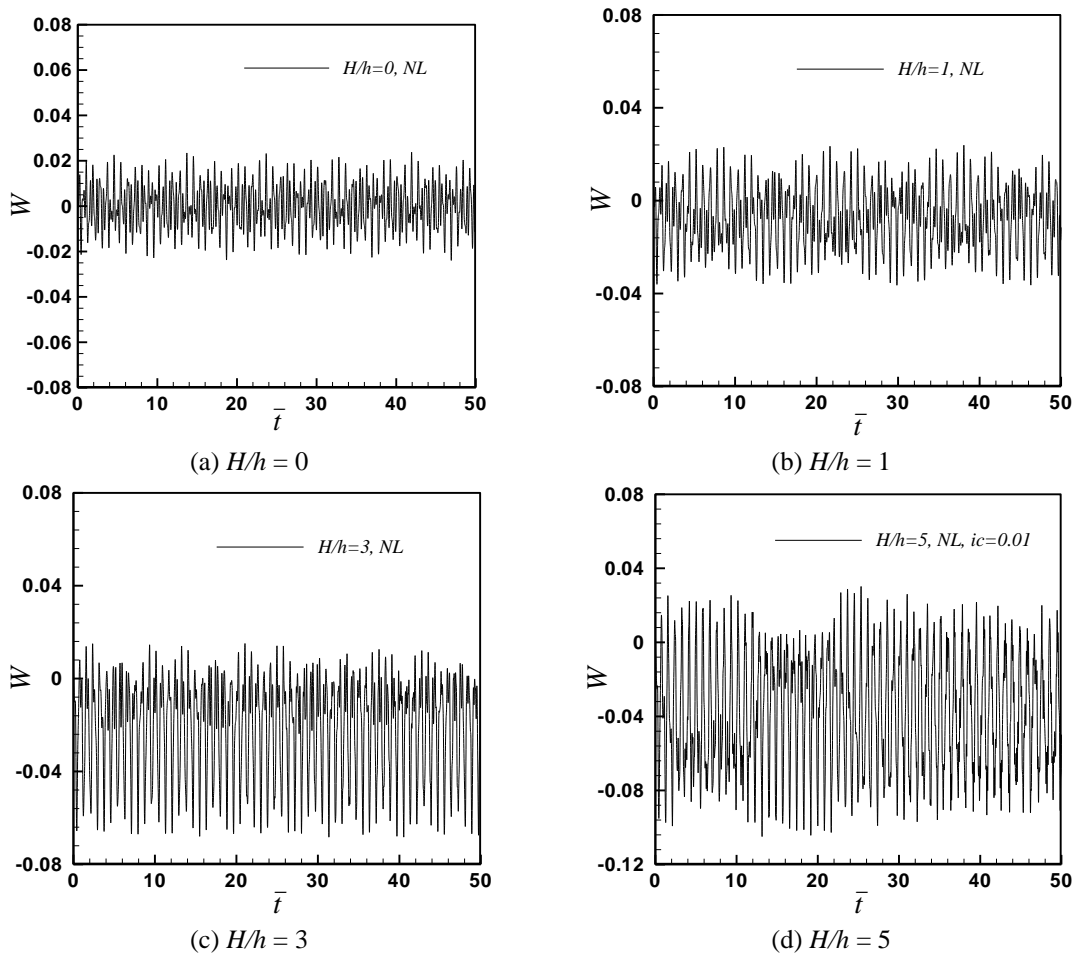
Fig. 9 Nonlinear plate vibration with the curvatures 0 to 5 and the initial condition 0.01

(c) *H/h = 1*   (d) *H/h = 5*
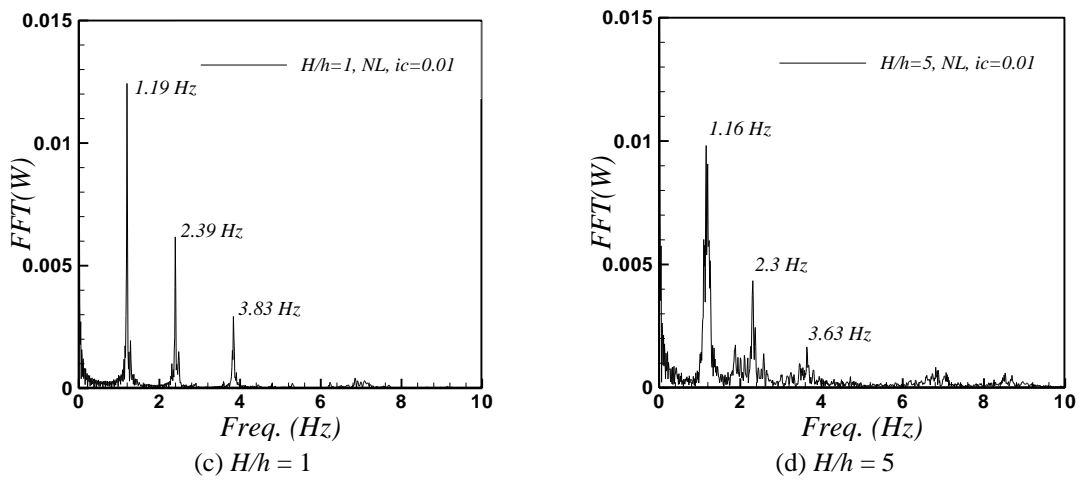
Fig. 10 Nonlinear frequency of curved plate with the curvatures 1 and 5 and the excitation 0.01

(a) curvature 1

(b) curvature 4
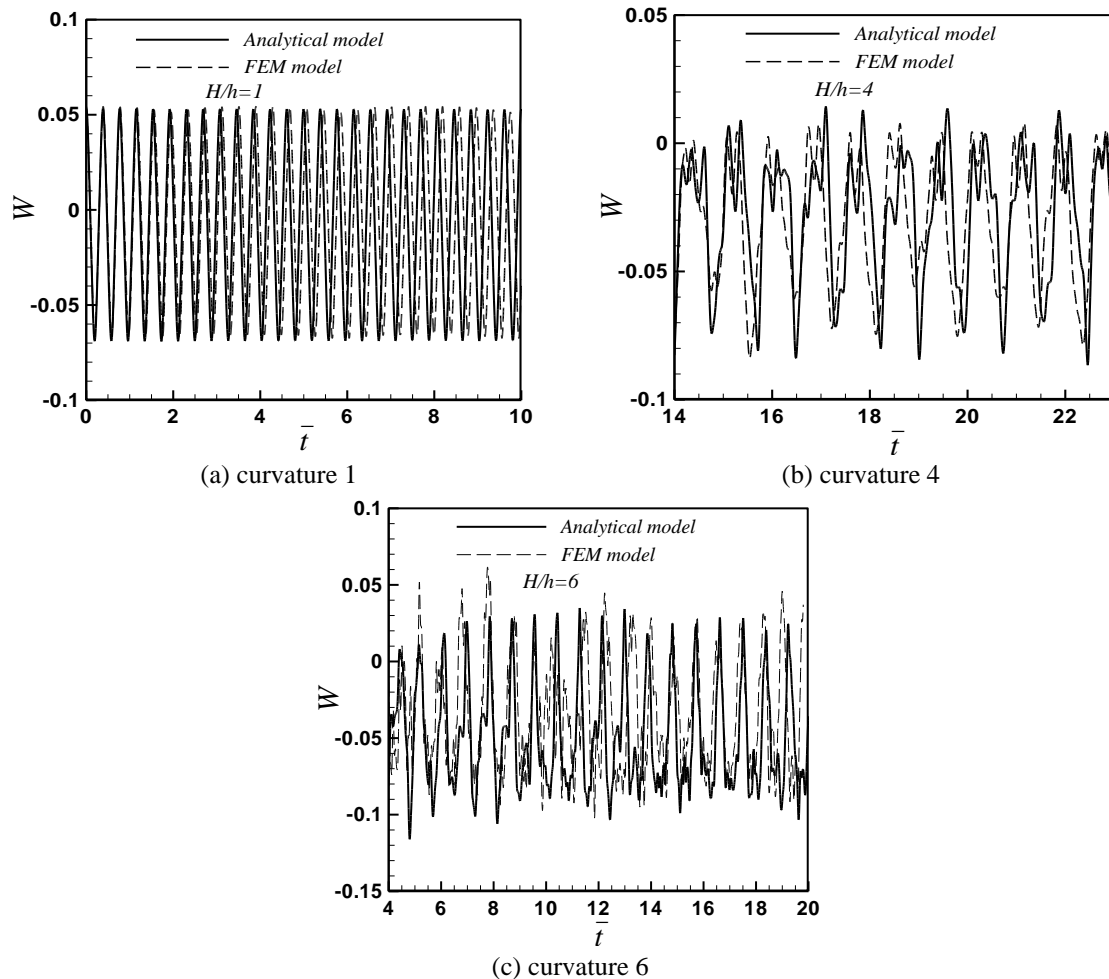
(c) curvature 6

Fig. 11 Comparison of curved plate oscillation amplitude with different curvatures using finite element and Galerkin methods

amplitude grows and becomes asymmetric. It also changes from a regular to an irregular oscillation.

Fig. 10 shows the nonlinear frequencies of the plate with the curvatures 1 and 5 for an excitation of 0.01. As the curvature increases, the frequencies exhibit no considerable variation and remain comparable. However, the excitation of the frequency range for curvature 5 is greater.

Figs. 11(a)-(c) respectively compare the oscillating behavior of a nonlinear curved plate with the curvatures 1, 4 and 6 using the nonlinear finite element and Galerkin methods with a specific excitation coefficient to determine the dynamic behavior. Fig. 11(a) shows the regular oscillating behavior of the plate for the curvature 1, indicating a very good agreement between the analytical and numerical results. In Figs. 11(b) and 11(c), the oscillations of the plate with the curvatures 4 and 6 are investigated, also exhibiting a very good agreement between the vibrational behavior in both numerical and semi-analytic analysis of Galerkin method. Both cases demonstrate chaotic behaviors of the system.
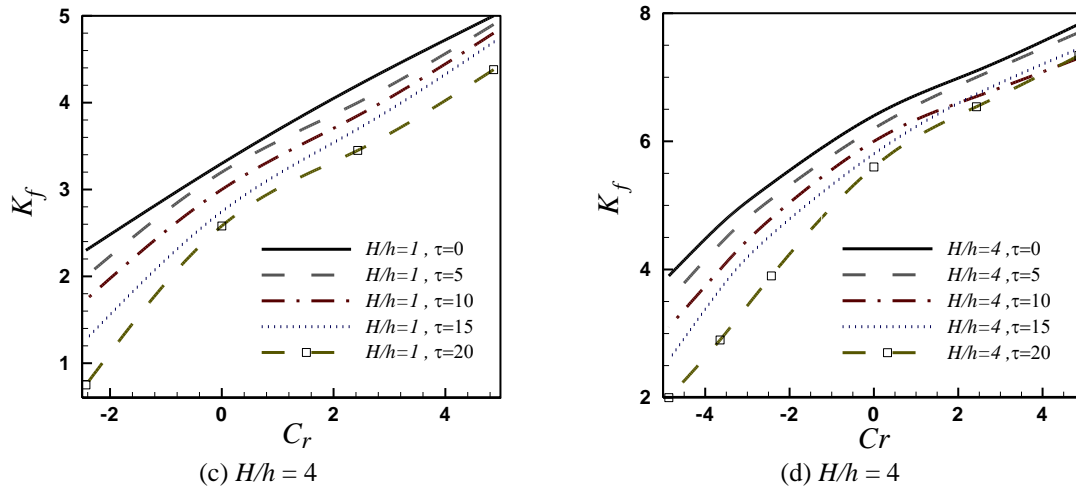
Fig. 12 Flutter frequency, K_f, versus in-plane load, C_r, for different thermal loads, τ

4.2 Aero-thermo-elastic analysis of the curved plate

The frequency of the curved plate flutter is investigated for different curvature ratios by changing the expressions of the in-plane load and the temperature of the plate surface in the frequency domain solution. In this section, some general results are discussed as follows.

For the curvatures 1 to 4:

(A) By changing the in-plane load from tension to compression, the flutter frequency decreases. (B) As the temperature inside the plate increases, the flutter frequency decreases due to the aerodynamic heating. (C) With increasing plate curvature, the flutter frequency increases. (D) A growth in the mechanical compressive load and aerodynamic heating, the decrease in the system flutter frequency occurs with a more negative slope. (F) By changing the tensile load to compression, the effect of thermal load on the flutter frequency reduction becomes more evident.

In Fig. 12(a), the effects of in-plane load and plate temperature on the flutter frequency are shown for the camber ratio 1. A large reduction in flutter frequency is exhibited with increasing in-plane compressive load. The flutter frequency is further decreased with increasing temperature.

The effect of in-plane load on the linear flutter frequency reduction for the camber ratio of 4 is depicted in Fig. 12(b). It is evident that the reduction in flutter frequency is more pronounced at a higher camber ratio.

To have a clear and accurate view of the complex behavior of the aeroelastic system, the non-dimensional flutter and divergence dynamic pressure boundary with respect to in-plane load for different thermal loads are also presented.

Some specific results observed in Figs. 13 and 14 are detailed as follow.

(a) The stability domain is small for the camber ratios 1 to 2, while it becomes larger for the camber ratios between 3 and 5. The stability domain for the camber ratio 6 shrinks.

(b) The boundaries of flutter and divergence are very sensitive to the variations in camber ratio, and a sudden change in plate aeroelastic instability behavior is observed.

Fig. 13(a) shows the static divergence of the panel for the camber ratio 1 and $C_r = -2$. The panel instability boundary is changed to flutter with increasing in-plane load ($C_r > -2$). For larger

(a) *H/h* = 1   (b) *H/h* = 1.5
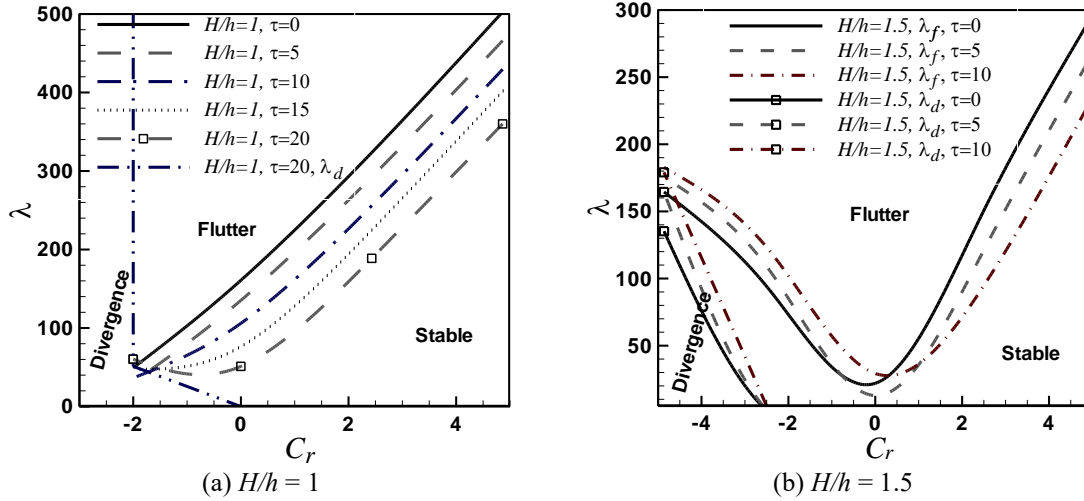
Fig. 13 Non-dimensional dynamic pressure, λ , versus in-plane load coefficient, C_r, for different thermal load coeffiencents τ

(a) *H/h* = 3   (b) *H/h* = 4
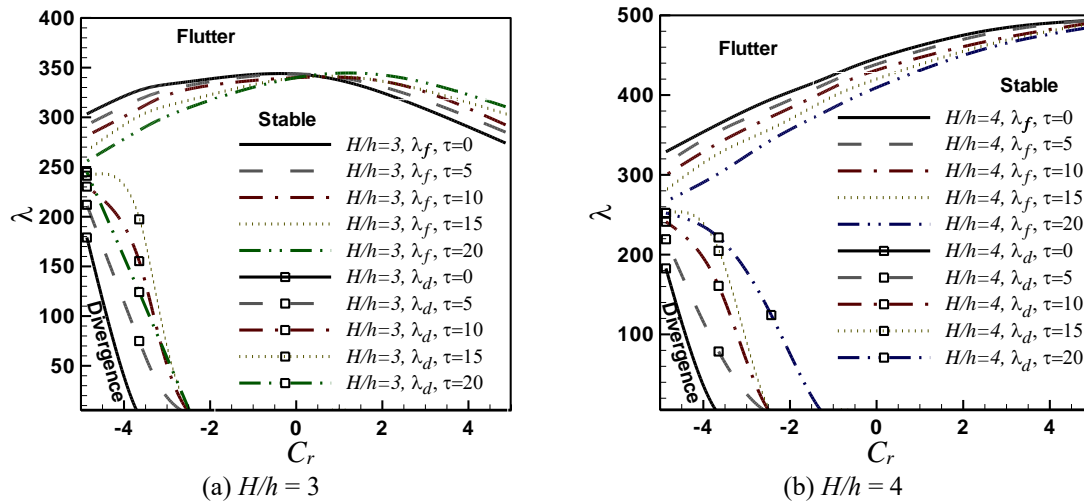
Fig. 14 Non-dimensional dynamic pressure, λ, versus in-plane load coefficient, C_r, for different thermal load coefficents τ

values of λ and larger thermal load coefficients (τ), the flutter boundary increases. For zero thermal load case ($\tau = 0$), the variation of flutter boundary with respect to in-plane load is linear while nonlinearity is observed for other thermal loads. λ_f

Fig. 13(b) shows that the flutter and divergence dynamic pressure (λ_f, λ_d) decrease with increasing C_r values between -5 and 0 for the camber ratio 1.5. A further increase in C_r reverses the flutter boundary. With increasing τ from 0 to 10 for a fixed non-dimensional dynamic pressure, the flutter instability boundary decreases for C_r values between -5 and 0, then increases for C_r values between 0 and 5. The divergence boundaries increase for C_r values between -5 and 0 and increasing τ from 0 to 10. A further growth in C_r reverses the flutter boundary.
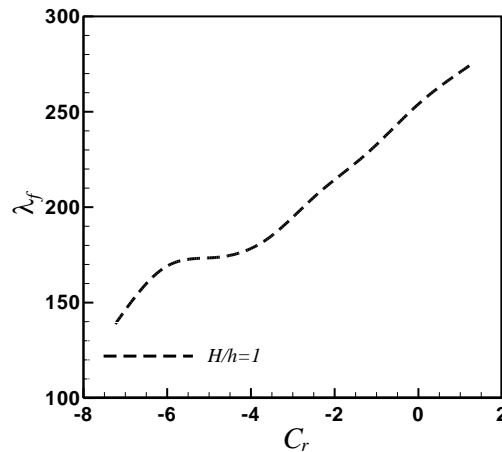
Fig. 15 Non-dimensional flutter dynamic pressure of the curved plate with the curvature 1 in terms of in-plate load

Fig. 14(a) shows that λ_d declines with increasing in-plane load for the camber ratio 3. However, λ_f boundary increases with increasing in-plane load from −5 to 0 and decreases with increasing in-plane load from 0 to 5. With increasing thermal load coefficient from 0 to 20 for a fixed λ, the panel divergence instability boundary increases. With increases λ for a fixed compressive load, the thermal load increases the flutter boundary and vice versa.

Fig. 14(b) shows that λ_d is reduced with increasing in-plane load for the camber ratio 4. In contrast, λ_f boundary increases with increasing in-plane load. With increasing thermal load coefficient from 0 to 20 for a fixed λ, the panel divergence instability boundary increases. With increasing thermal load coefficient for a fixed in-plane load, the flutter boundary decreases. With increasing compressive in-plane load, the flutter and divergence boundaries converge. According to the results, with increasing value of in-plane load, the flutter boundaries for different thermal load coefficients converge.

The combination of curvature with a constant in-plane load is influential in the regular and irregular behaviors as well as in the amplitude of plate vibrations.

Fig. 15 shows the dynamic pressure of a nonlinear curved plate flutter with the curvature 1 in terms of increasing compressive in-plane load. As the in-plane load increases, the flutter velocity decreases continuously and remains almost constant for the coefficients −4 to −6. Therefore, the compressive force inside the plate brings about the aeroelastic instability of this flutter type for the curved plate with a curvature of 1. A comparison of the changes of flutter boundary in the nonlinear analysis of time domain (Fig. 15) with the linear analysis of frequency domain (Fig. 13(a)) is also carried out. One observes that changing the in-plane load coefficient from 1 to 0 and −2 in the frequency analysis decreases the flutter velocity from 220 to 180 and 60. In the nonlinear analysis, however, the flutter velocity changes from 270 to 250 and 220. Therefore, the decrease in the flutter velocity occurs much more slowly in the nonlinear analysis, and the nonlinear terms of the structural equations increase the flutter boundary and structural stability.

Figs. 16(a) and 16(b) show the oscillation amplitude and frequency of the curved plate flutter with a curvature of 1 in terms of in-plane load for dimensionless dynamic pressure 275. As the flutter oscillation amplitude of the curved plate increases, the flutter frequency decreases.

(a) Nondimensional flutter oscillation amplitude

(b) Non-dimensional flutter frequency
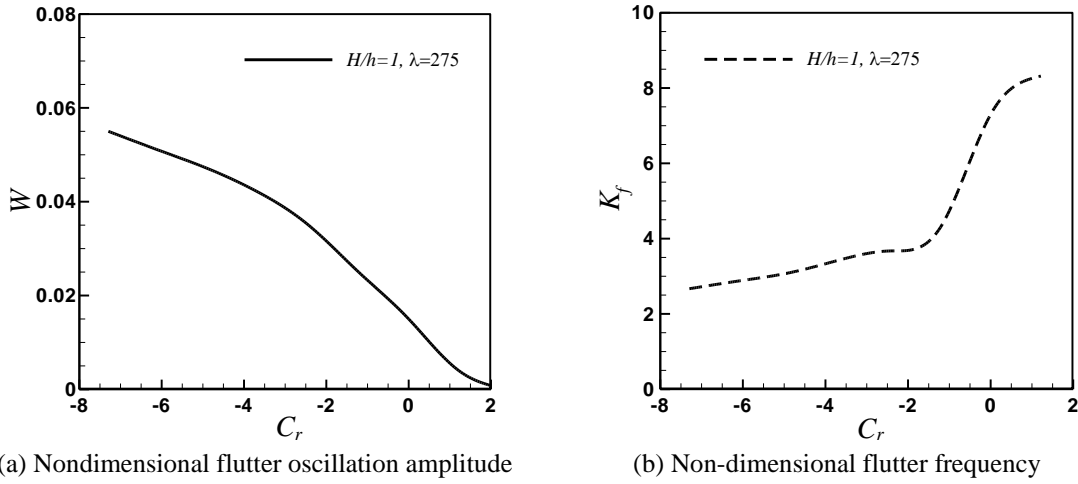
Fig. 16 Oscillation amplitude and frequency of the curved plate with the curvature 1 in terms of in-plane compressive load for the dynamic pressure 275

(a) Curvature 1
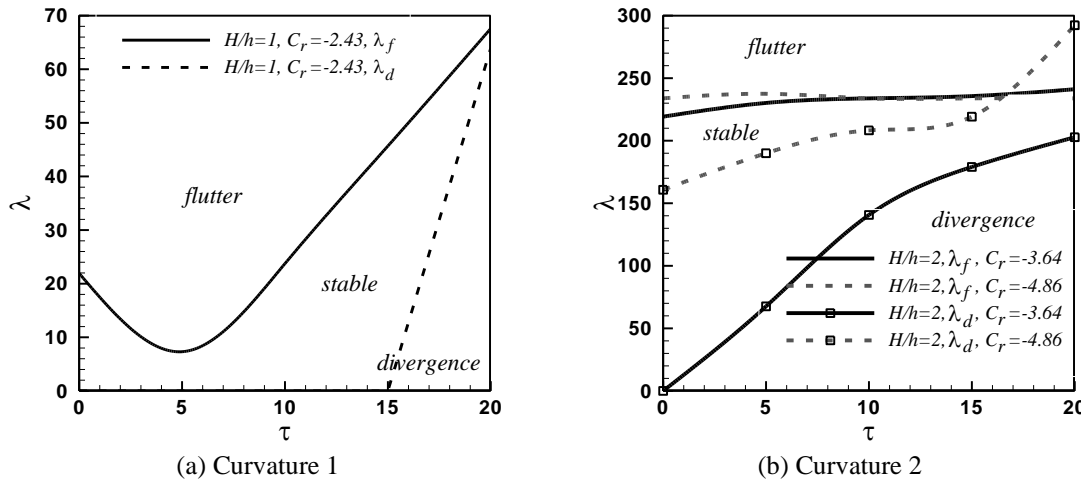
(b) Curvature 2

Fig. 17 Stability, flutter, and divergence range of the plate based on dimensionless dynamic pressure in terms of heat for a given compressive load

Therefore, with increasing compressive force for a curvature of 1, while the oscillation amplitude grows, the flutter frequency decreases and the structure behavior softens.

The curvature effect exhibits special and distinct changes in the analysis of flutter phenomenon. In fact, the effects of plate curvature and aerodynamic loading creates a complex combination, and the results include certain subtleties. Figs. 17 and 18 show the range of plate stability, flutter, and divergence. The dimensionless dynamic pressure diagram in terms of temperature is also plotted for different curvatures and in-plane loads. Several general results can be obtained. (A) For a certain amount of in-plane load, by increasing the curvature of the plate from 1 to 4, an increase in the stability range can be observed. (B) At the curvature ratio of 1 for the compressive force coefficient of −2.43, the divergence region of the small plate resides in the temperature range of 16 to 20 and the dynamic pressure is 0 to 60. By increasing the plate curvature to 2–4, while the

(a) Curvature 3   (b) Curvature 4
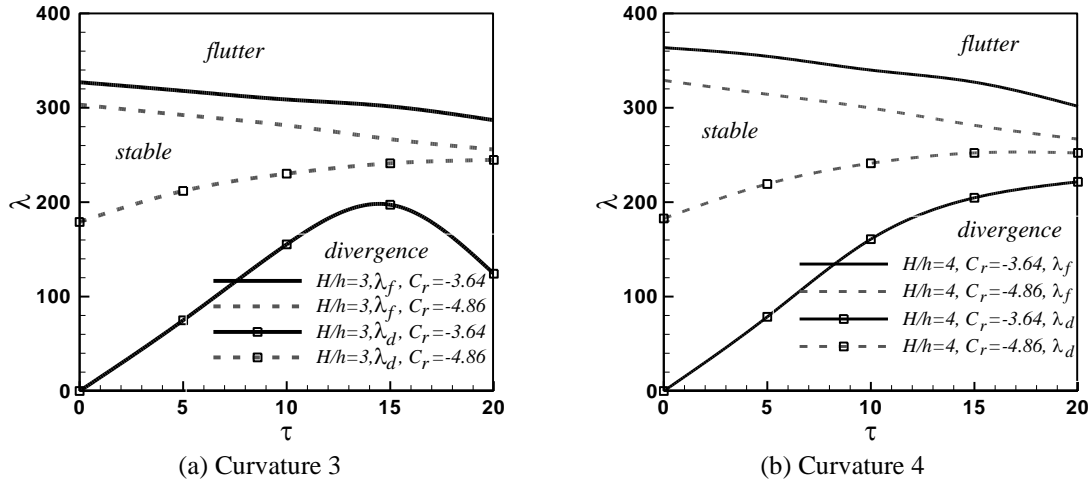
Fig. 18 Stability, flutter, and divergence range of the curved plate based on the dimensionless dynamic pressure in terms of heat for a given compressive load

(a) Frequency map   (b) Damping map
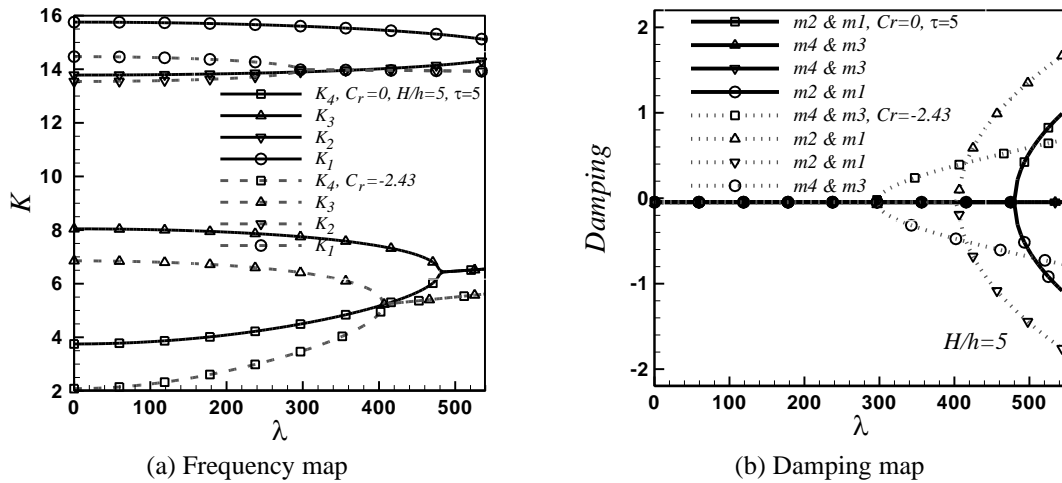
Fig. 19 Frequency and damping diagrams of the plate with the curvature 5 and the conditions of combination of higher modes

compressive force coefficient is -3.64, the divergence region is quite large and almost similar. (C) For the curvatures 2 to 4, with increasing plate curvature, the flutter boundary shifts to a higher dynamic pressure and the stability zone expands. (D) with increasing curved plate temperature, the stability zone shrinks (One should note that for the curvature 3, compressive force coefficient -4.86, and growing temperature to more than 15, the divergence zone decreases unlike higher curvatures and the stability zone becomes larger).

Figs. 19(a) and 19(b) show the frequency and damping diagram of the system in terms of dimensionless dynamic pressure, in the eigenvalue analysis, for the curvature 5 and force coefficients of 0 and -2.43. For a force coefficient of 0, the flutter occurs at the dynamic pressure of 470. For a compressive load factor of -2.43, the third and fourth modes at a dynamic pressure of 300 are combined to show the plate flutter. Therefore, increasing the plate curvature results in
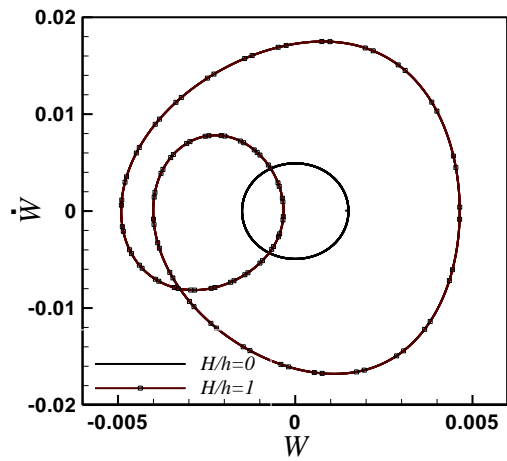
(a) Curvatures 0 and 1, first-order piston theory
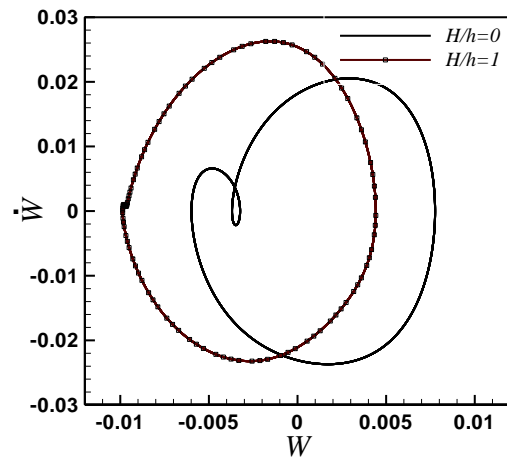
(b) Curvature 0 and 1, third-order piston theory
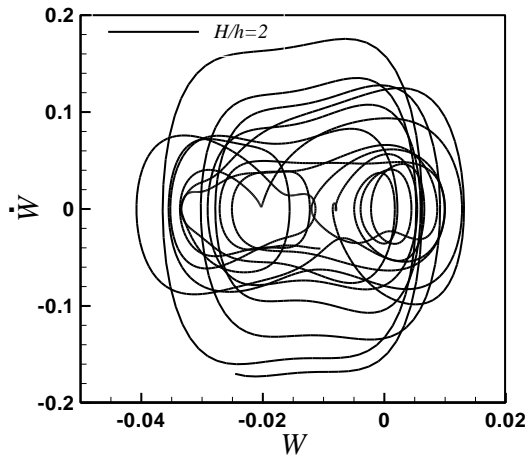
(c) Curvature 2
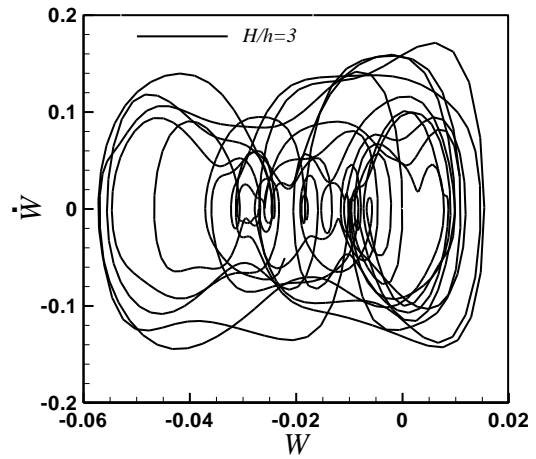
(d) Curvature 3
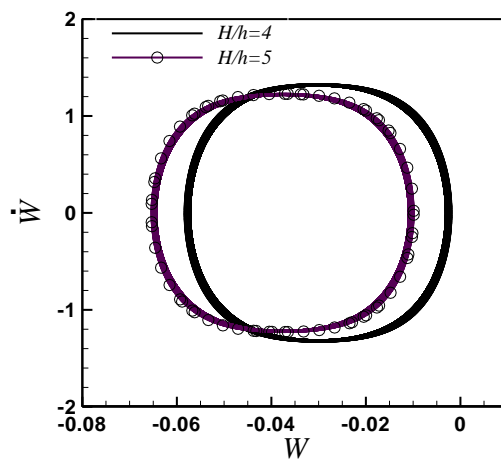
(e) curvature 4 and 5

Fig. 20 Limited and turbulent curved plate oscillation for *H/h* 0 to 5, using first- and third-order piston theory
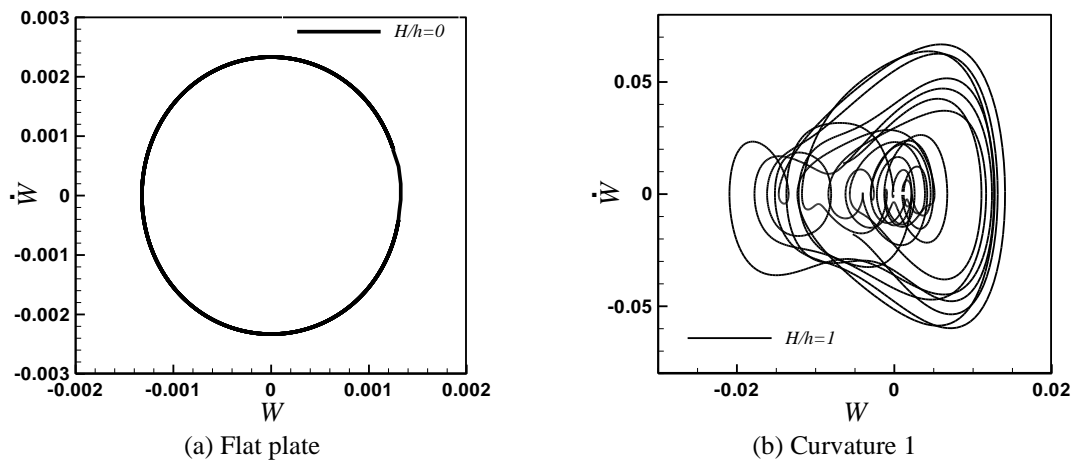
(a) Flat plate   (b) Curvature 1

Fig. 21 LCO and turbulent behavior of flat and curved plates with the effect of in-plane load factor −2.43

an earlier occurrence of stimulation and combination of higher modes than those observed at lower modes while reducing the flutter boundary.

The analysis of the aeroelastic behavior of the curved plate is investigated by changing the curvature and the effect of in-plane and thermal load on the plate. Figs. 20(a) and 20(b) show the LCO behavior of the flat and curved plate ($H/h = 1$) using the first- and third-order piston theory, respectively. For both plates, the flutter behavior is LCO, although the finite cycle shape has changed according to the plate curvature and aerodynamic theory. The range of fluctuations for both theories is almost in the same range. For the curvature 1, two-period behavior is observed using the first-order piston theory and one-period behavior is observed using the third-order piston theory.

Figs. 20(c) and 20(d) show the chaotic behavior of the plate with the curvatures 2 and 3, respectively. As the plate curvature grows, the oscillation amplitude increases. Furthermore, as the plate curvature increases to 4 and 5, the oscillation amplitude grows, while the structural behavior finds the form of a fixed finite cycle oscillation band.

Figs. 21(a) and 21(b) show the LCO of flat plate and the chaotic behavior of curved plate for a curvature 1 considering the effect of a compressive load factor −2.43. For a curved plate of curvature 1, with increasing in-plane load from 0 to −2.43, the system behavior changes from LCO to chaotic. The fluctuation range also increases.

Fig. 22(a) shows the panel flutter dynamic pressure versus panel camber ratio obtained using the first-order piston theory (PTA1) and third-order piston theory (PTA3). With increasing panel curvature, λ_f is reduced. With the use of PTA1, λ_f decreases from 350 (flat panel) to 80 (curved panel with the camber ratio of 5). This clearly emphasizes that PTA3 reduces the flutter dynamic pressure. This reduction is more significant for the flat panel at higher dynamic pressures. With increasing panel camber ratio, λ_f decreases and the dynamic pressure difference between PTA1 and PTA3 decreases and vanishes.

Fig. 22(b) shows the panel flutter dynamic pressure versus panel camber ratio found using PTA1 and PTA3. Simulations are conducted for $\tau = 5$, $\delta_e = 1$ and $\delta_\alpha = 1$ in this case. With increasing panel camber ratio to 1 for PTA1, λ_f is reduced from 300 (flat panel) to 180, then increase to 230 for a camber ratio of 1.5. As the camber ratio increases from 1.5 to 5, λ_f decreases to 70. This clearly shows that PTA3 reduces the flutter dynamic pressure although the trend of
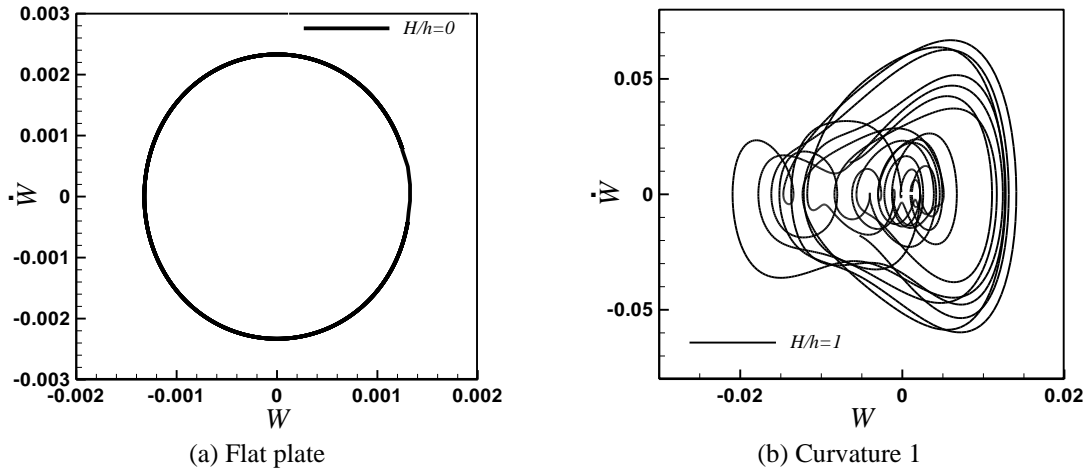
(a) Flat plate   (b) Curvature 1

Fig. 21 LCO and turbulent behavior of flat and curved plates with the effect of in-plane load factor −2.43

(a) Zero in-plane load   (b) Thermal load effect

(c) In-plane load effect   (d) Thermal load with thermal-dependent material
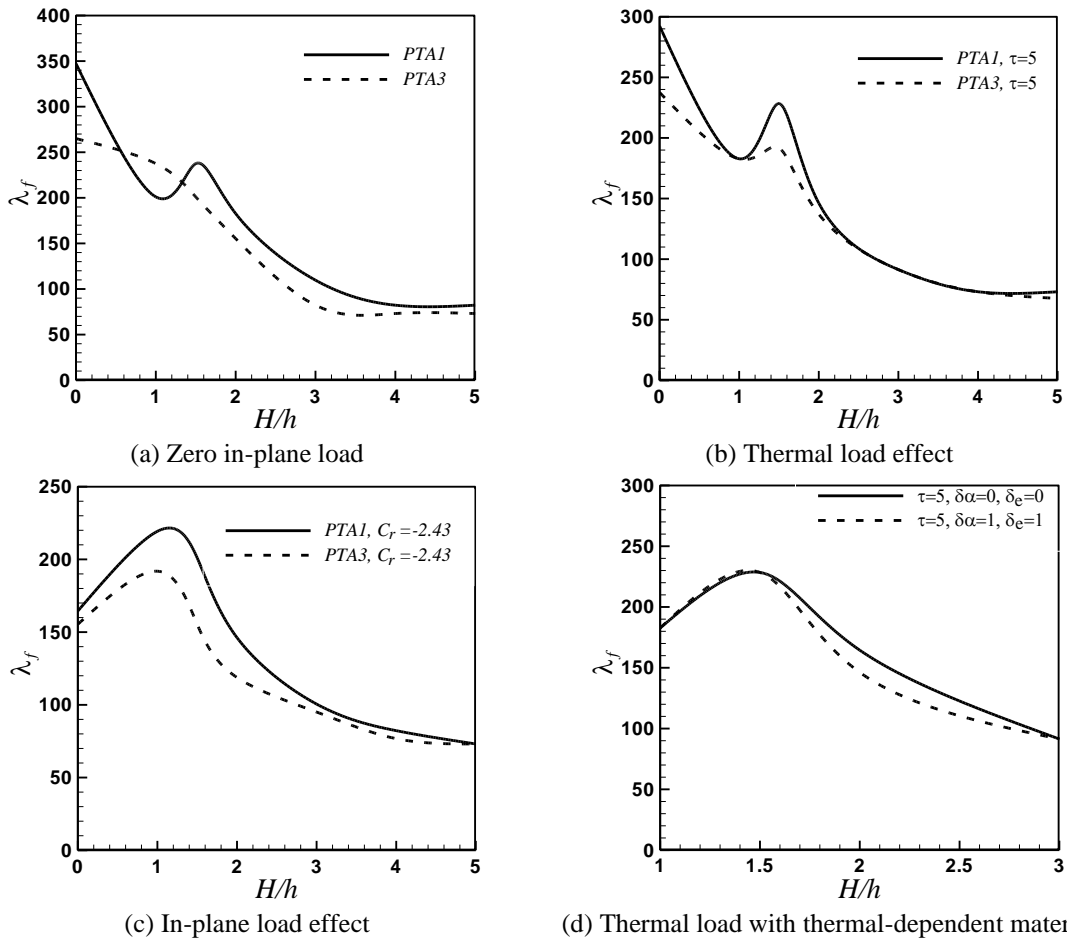
Fig. 22 Comparison of flutter dynamic pressure in terms of curvature for the first- and third-order piston theory

flutter dynamic pressure variation is similar. One concludes that the thermal load decreases λ_f with respect to the camber ratio.

Fig. 22(c) shows the panel flutter dynamic pressure versus panel camber ratio found using PTA1 and PTA3. Simulations for this case are conducted for the in-plane load effect ($C_r = -2.43$). With increasing panel camber ratio up to 1, λ_f increases from 160 to 230 based on PTA1, and with increasing panel camber ratio from 1 to 5, λ_f decreases to 70. It is evident that with the use of PTA3 instead of PTA1, the flutter dynamic pressure decreases. On the contrary, with increasing panel camber ratio from 0 to 5, the difference between PTA1 and PTA3 diminishes. By considering the effect of mechanical in-plane load, the variation of flutter dynamic pressure with respect to panel camber ratio changes alongside Figs. 22(a) and 22(b) with and without thermal effects.

Fig. 22(d) highlights the impact of temperature in conjunction with the thermal degradation of the thermo-mechanical properties of panel material on the flutter dynamic pressure. With increasing panel curvature, the temperature dependency of structural properties leads to a reduction in the dynamic pressure instability. For a camber ratio of 2, the maximum difference between λ_f of thermal-dependent and thermal-independent materials is shown.

5. Conclusions

The supersonic flutter behavior of 2D curved panels is studied using the Galerkin method which considers the structural nonlinearities. Numerical studies of the aero-thermo-elastic system including curvature ratio, in-plane load, thermal load distribution on the panel as a function of length, thickness ratio, temperature dependency of material properties, first and third order piston theory, and the structural analysis in the frequency and time domain approaches are conducted. The following results are obtained.

In the frequency domain:

(1) Structural frequency reduction is dependent on thermal effects. (2) Temperature dependent materials can decrease the structural frequency. (3) Compressive load reduces the structural frequency and buckling load. (4) With increasing in-plane tensile load at the boundaries, λ_f increases. (5) With increasing in-plane temperature, λ_f decreases. (6) With increasing in-plane compressive load, the panel flutter frequency decreases continuously. (7) With increasing thermal and in-plane loads, divergence becomes more critical. (8) With increasing panel curvature, structural and panel flutter frequencies increase. (9) With an increase in panel curvature, the structural stability domain shifts from higher to lower temperature. (10) With increasing plate camber, stability increases. (11) For curved panels, at low values of λ and high temperatures, divergence conditions are observed more frequently. For high values of λ in different temperature regions, the flutter is observed more recurrently. (12) With increasing panel curvature to higher ratios ($H/h > 4$), there is an increase of higher mode combinations and lower λ_f. (13) A complicated unstable aeroelastic behavior of the panel is observed with the combined effects of higher panel curvatures, in-plane loads and heat.

In the time domain:

A nonlinear analysis is performed in the time domain to study the vibration and flutter behavior.

(1) As the plate curvature grows, the frequencies of linear structure increase. The nonlinear frequencies of the first to third modes increase slightly for a curvature ratio of less than 3, then

decreases to some extent. In general, the plate frequency variations in the nonlinear analysis are much more limited than those observed in the linear mode. 2) As the plate curvature increases from 0 to 3, the phase diagram changes from LCO to chaotic motion, and a further increase in curvature exhibits a definite band of LCO. 3) With increasing compressive load in the plate, the oscillation amplitude increases and the flutter frequency decreases, demonstrating a softness in the structural behavior. (4) Based on the third-order piston theory, the flutter boundary is more critical than that observed for the first-order piston theory. 5) As the plate curvature increases, the flutter velocity decreases and the results of the first- and third-order piston theory converge. 6) By increasing the plate curvature to the values of 4 and 5, the flutter velocity becomes almost uniform.

References

Abbas, L.K., Rui, X., Marzocca, P., Abdalla, M. and De Breuker, R. (2011), "A parametric study on supersonic/hypersonic flutter behavior of aero-thermo-elastic geometrically imperfect curved skin panel", *Acta Mechanica*, **222**(1), 41-57. https://doi.org/10.1007/s00707-011-0525-8.

Amirzadegan, S., Safavi, S.M.M. and Jafarzade, A. (2019), "Supersonic panel flutter analysis assuming effects of initial structural stresses", *J. Inst. Eng. India Ser. C*, **100**(5), 833-839. https://doi.org/10.1007/s40032-019-00532-y.

Amirzadegan, S. and Dowell, E.H. (2020), "Nonlinear limit cycle oscillation and flutter analysis of clamped curved plates", *J. Aircraft*, **57**(2), 368-376. https://doi.org/10.2514/1.C035716.

Azzouz, M.S., Przekop, A., Guo, X. and Mei, C. (2003), "Nonlinear flutter of shallow shell under yawed supersonic flow using FEM", *Proceedings of the 44th AIAA/ASME/ASCE/AHS/ASC Structures*, *Structural Dynamics*, *and Materials Conference*, Virginia, U.S.A., April.

Azzouz, M., Guo, X., Przekop, A. and Mei, C. (2004), "Nonlinear flutter of cylindrical shell panels under yawed supersonic flow using FE", *Proceedings of the 45th AIAA/ASME/ASCE/AHS/ASC Structures*, *Structural Dynamics & Materials Conference*, California, U.S.A., April.

Azzouz, M. and Mei, C. (2005), "Nonlinear flutter of cylindrical panels under yawed supersonic flow using finite elements", *Proceedings of the 46th AIAA/ASME/ASCE/AHS/ASC Structures*, *Structural Dynamics and Materials Conference*, Texas, U.S.A., April.

Azzouz, M. (2009), "Flow angle effects on supersonic flutter of clamped curved panels", *Proceedings of the 50th AIAA/ASME/ASCE/AHS/ASC Structures*, *Structural Dynamics*, *and Materials Conference 17th AIAA/ASME/AHS Adaptive Structures Conference 11th AIAA*, California, U.S.A., May.

Birman, V., Bert, C.W. and Elishakoff, I. (1990), "Effect of aerodynamic heating on deformation of composite cylindrical panels in a gas flow", *Compos. Struct.*, **15**(3), 259-273. https://doi.org/10.1016/0263-8223(90)90034-C.

Cao, L., Yao, G. (2019), "Hopf bifurcation of heated panels flutter in supersonic flow", *Mathematics*, **7**(9), 787. https://doi.org/10.3390/math7090787.

Epureanu, B.I., Tang, L.S. and Païdoussis, M.P. (2004), "Coherent structures and their influence on the dynamics of aeroelastic panels", *Int. J. Non Linear Mech.*, **39**(6), 977-991. https://doi.org/10.1016/S0020-7462(03)00090-8

Fazelzadeh, S.A. (2007), "Chaotic behavior of nonlinear curved-panel in a supersonic flow", *Dynam. Cont. Dis.Ser. B*, **14**(6), 793.

Gee, D.J. and Sipcic, S.R. (1999), "Coupled thermal model for nonlinear panel flutter", *AIAA J.*, **37**(5), 642-650. https://doi.org/10.2514/2.765.

Ghoman, S., Azzouz, M. and Mei, C. (2009), "Time domain method for nonlinear flutter of curved panels under yawed supersonic flow at elevated temperature", *Proceedings of the 50th AIAA/ASME/ ASCE/AHS/ASC Structures*, *Structural Dynamics*, *and Materials Conference 17th AIAA/ASME/AHS Adaptive Structures Conference 11th AIAA No* (p. 2598), California, U.S.A., May.

Kouchakzadeh, M.A., Rasekh, M. and Haddadpour, H. (2010), "Panel flutter analysis of general laminated composite plates", *Compos. Struct.*, **92**(12), 2906-2915. https://doi.org/10.1016/j.compstruct.2010.05.001.

Krause, H. and Dinkler, D. (1998), "The influence of curvature on supersonic panel flutter", *Proceedings of the 39th AIAA/ASME/ASCE/AHS/ASC Structures*, *Structural Dynamics*, *and Materials Conference and Exhibit*, Califirnia, U.S.A., April

Librescu, L., Marzocca, P. and Silva, W.A. (2002), "Supersonic/hypersonic flutter and postflutter of geometrically imperfect circular cylindrical panels", *J. Spacecraft Rockets*, **39**(5), 802-812. https://doi.org/10.2514/2.3882.

Miller, B.A., McNamara, J.J., Spottswood, S.M. and Culler, A.J. (2011), "The impact of flow induced loads on snap-through behavior of acoustically excited, thermally buckled panels", *J. Sound Vib.*, **330**(23), 5736-5752. https://doi.org/10.1016/j.jsv.2011.06.028.

Muc, A., Flis, J. and Augustyn, M. (2019), "Optimal design of plated/shell structures under flutter constraints—A literature review", *Materials*, **12**(24), 4215. https://doi.org/10.3390/ma12244215.

Nydick, I., Friedmann, P. and Zhong, X. (1995), "Hypersonic panel flutter studies on curved panels", *Proceedings of the 36th Structures*, *Structural Dynamics and Materials Conference*, Los Angeles, U.S.A., April.

Pany, C. and Parthan, S. (2003), "Flutter analysis of periodically supported curved panels", *J. Sound Vib.*, **267**(2), 267-278. https://doi.org/10.1016/S0022-460X(02)01493-1.

Reddy, J.N. (2003), *Mechanics of Laminated Composite Plates and Shells: Theory and Analysis*. CRC press.

Singha, M.K. and Mandal, M. (2008), "Supersonic flutter characteristics of composite cylindrical panels", *Compos. Struct.*, **82**(2), 295-301. https://doi.org/10.1016/j.compstruct.2007.01.007.

Yang, C., Li, G. and Wan, Z. (2012), "Aerothermal-aeroelastic two-way coupling method for hypersonic curved panel flutter", *Sci. China Technol. Sci.*, **55**(3), 831-840. https://doi.org/10.1007/s11431-011-4722-4.

Yang, T.Y. and Han, A.D. (1976), "Flutter of thermally buckled finite element panels", *AIAA J.*, **14**(7), 975-977. https://doi.org/10.2514/3.7173.

Zhou, X., Wang, L., Jiang, J., Su, Z. (2019), "Hypersonic aeroelastic response of elastic boundary panel based on a modified fourier series method", *International Journal of Aerospace Engineering*, **13**, 5164026. https://doi.org/10.1155/2019/5164026.

EC

Nomenclature

panel thickness	h
curvature height	$\hat{h}$
curvature changes	H/h
out-of-plane displacement	w_0
plate width	a
tension or compression force coefficient	η
plate stiffness	D

elastic modulus	E
Poisson's ratio	V
radii of curvature	$\underline{R}_x$
aerodynamic pressure	ΔP_a
dynamic flow pressure above the plate	P^d
Low static pressure	P^s
speed of sound	c_∞
Free-stream steady velocity	U_∞
virtual strain energy	δU
virtual work	δV
virtual kinetic energy	δK
stress tensor	$\vec{\vec{\sigma}}$
strain tensor	$\vec{\vec{\varepsilon}}$
external distributed force vector	$\vec{\mathbf{p}}$
displacement vector	$\vec{\mathbf{u}}$
velocity vector	$\vec{\mathbf{u}}_{,t}$
in-plane axial force resultant	N_x
in-plane thermal force resultant	N_x^T
bending moments resultant	M_x
thermal moments resultant	M_x^T
modulus of elasticity and thermal expansion	δ_e , δ_α
rise in plate temperature	ΔT
free stream temperature	T

atmospheric pressure	P_∞
plate density	ρ_m
air density	ρ_∞
isentropic gas constant	γ
Mach number	M
dynamic pressure	q_∞
comparison functions	$\phi_r(\xi)$
non-dimensional frequencies	K
reference temperature	T_{ref}
maximum in-plane temperature	T^*
thermal variation coefficients for E	e_T
thermal variation coefficients for α	α_T
thermal expansion coefficient	α
in-plane load coefficient	C_r
magnitude of in-plane load	R_x
first frequency	Ω_0
non-dimensional frequency	$\bar{\Omega}$